



# CHORUS

This is the accepted manuscript made available via CHORUS. The article has been published as:

## Disentangling photoexcitation and photoluminescence processes in defective MgO

Christian Vorwerk and Giulia Galli

Phys. Rev. Materials **7**, 033801 — Published 28 March 2023

DOI: [10.1103/PhysRevMaterials.7.033801](https://doi.org/10.1103/PhysRevMaterials.7.033801)

# Disentangling Photoexcitation and Photoluminescence Processes in defective MgO

Christian Vorwerk\*

*Pritzker School of Molecular Engineering, University of Chicago, Chicago IL 60637, USA*

Giulia Galli†

*Pritzker School of Molecular Engineering and Department of Chemistry,  
University of Chicago, Chicago IL 60637, USA and*

*Materials Science Division and Center for Molecular Engineering,  
Argonne National Laboratory, Lemont IL 60439, USA*

(Dated: March 13, 2023)

Oxygen vacancies are ubiquitous in oxides and strongly influence the material’s electronic structure and catalytic and transport properties. Here we focus on a seemingly simple defective oxide, MgO, and on the electronic properties of oxygen vacancies, which remain controversial in spite of numerous studies. We present an *ab initio* investigation of the photoexcitation and photoionization process of these defects, using a newly developed embedding Bethe-Salpeter equation approach, implemented in the WEST code. We find absorption and emission energies in good agreement with experiments. Our results provide a detailed, microscopic understanding of the absorption and emission processes of the neutral and positively charged oxygen vacancy, reconciling different views present in the chemistry and condensed-matter physics communities.

## I. INTRODUCTION

Oxygen vacancies are abundantly present in all metal oxides and profoundly influence their properties [1]. In particular, in the case of magnesium oxide (MgO) oxygen vacancies play a key role when using the material in spintronic devices [2–5] or as a substrate for heterogeneous catalytic processes [6–10]. Therefore, the electronic structure of the oxygen vacancy ( $V_O$ ) in MgO has been extensively studied in the last decade, for example by using a variety of *ab initio* theoretical methods, and it is found to be deceptively simple [10–18]: The missing oxygen gives rise to a *s*-like defect state in the band gap of the oxide, which is mostly localized in proximity of the empty lattice site. This defect state can be filled by 2 (neutral charge state  $V_O^0$ ), 1 (positive charge state  $V_O^+$ ), or 0 electrons (double positive charge state  $V_O^{2+}$ ). Additionally, the missing oxygen gives rise to a three-fold degenerate *p*-like state above the conduction band minimum (CBM) that is less localized than the mid-gap *s*-like state. Experimentally, it is well established that the neutral charge state absorbs light at 5.0 eV [19, 20], while the positive charge state absorbs at a slightly lower energy, 4.95 eV [19–21]. Emission from the neutral charge state has been observed at 2.4 eV [20] and for the positive charge state at 3.13–3.22 eV [19, 20].

Different theoretical studies not only disagree on the exact absorption and emission energies of the oxygen vacancy in MgO, but they also provide conflicting interpretations of the microscopic processes responsible for absorption and emission. The absorption of the neutral and positive charge states have been assigned either to photoionization processes, *i.e.*  $V_O^0 \rightarrow V_O^+ + e^-$  and  $V_O^+ \rightarrow V_O^{2+} + e^-$ , respectively, or to excitations of a specific defect charge state. The different interpretations originate from different scientific communities: Calculations using methods from solid-state physics, such as many-body perturbation theory [16, 17] and quantum monte-carlo [14], favor photoionization as the origin of the absorption processes. On the other hand, quantum-chemical methods, such as complete active space perturbation theory (CASPT2) [15] and equation-of-motion coupled cluster (EOM-CCSD) [13] favor defect excitations as the origin of the absorption. Similar disagreements exist for the emission process: While solid-state physics simulations attribute the emission to valence hole capture in the  $V_O^0$  defect, quantum-chemical calculations attribute the emission to spin-triplet defect de-excitations. To add to the difficulty in comparing results, simulations of the oxygen vacancy in MgO reported in the literature have used supercells or embedded clusters of different sizes, and it has been observed that excitation and emission energies converge slowly with supercell size. Some studies reported a  $N_{\text{atoms}}^{-1}$ -dependence of excitation energies, indicating that extrapolations to the dilute limit are necessary [13]. A summary of the results of relevant, previous calculations is provided in Table I.

In this study, we investigate the microscopic processes responsible for absorption and emission in MgO when oxygen vacancies are present, in the dilute limit. This endeavour requires a formalism that can accurately describe

---

\* vorwerk@uchicago.edu

† gagalli@uchicago.edu

Method	Structure	No. of atoms	Excitation	Ionization	Luminescence
EOM-CCSD@HF [13]	prim. s.c.	$\infty$	5.2	–	3.7
QMC@PBE [14]	conv. s.c.	63	–	5.0	4.1
CSPT2 [15]	emb. cluster	26-32	5.4	–	4.1
BSE-GW@PBE0 [16]	conv. s.c.	63	–	4.95	3.4
scGW [17]	prim. s.c.	53	–	5.2	–
G <sub>0</sub> W <sub>0</sub> [17]	prim. s.c.	53	–	4.48	–
TDDFT@PBE0 [18]	conv. s.c.	216 – 1000	4.85	–	2.0

TABLE I. Summary of the results of previous calculations for the photoexcitation, -ionization and -luminescence energies of the neutral oxygen vacancy in MgO. We report the structure and number of atoms in the supercell (abbreviated as s.c.)/cluster used in all calculations. All energies are in eV.

excitations between localized states as well as those from localized to delocalized states. Additionally, the formalism should account for the correlation between an excited electron and the hole created in the process, since the formation of strongly bound excitons has been reported for both pristine [22] and defective MgO [16]. Recent calculations combining the *GW* method to obtain quasi-particle energies with the solution of the Bethe-Salpeter equation (BSE) for neutral excitations have yielded accurate results for the excitation energies in bulk MgO [22], as well as for point defects in MgO [16] and other semiconductors [16, 23]. However, BSE calculations for the oxygen vacancy have only been performed for cells containing 63 atoms [16] due to the unfavourable scaling of BSE calculations with system size; in addition, in some cases, BSE calculations performed in large supercells could not identify specific defect excitation energies within the large number of computed excitations [23].

Here we employ an *embedded BSE* formalism [24], an approach based on many-body perturbation theory specifically designed to obtain defect excitation energies. In embedded BSE, the electron-hole correlation function is down-folded onto a properly chosen active space, formed by localized single particle orbitals. This procedure avoids the calculation of all excitation energies of the solid and focuses only on those of the defect, thus greatly reducing the computational cost. This formalism, which leads to the solution of a reduced BSE for the defect states and includes the screening of the environment, was originally suggested for spatially heterogeneous systems, such as 2D materials on substrates [24]. In our work, we present the first application of the method to defects in bulk semiconductors. Thanks to the reduced cost of solving the BSE, we could use much larger supercells than previously reported in the literature. In our work, we resolve the discrepancy between many body perturbation theory and quantum chemical calculations and we discuss a robust computational protocol that is general and can be applied to weakly correlated defects in semiconductor and insulators.

The rest of the paper is organized as follows: in section II we describe the methodology adopted in this work, including computational details. In section III we present our results and section IV summarizes and concludes the paper.

## II. METHODOLOGY

Neutral excitations occurring upon light absorption can be obtained from the solution of the Bethe-Salpeter Equation (BSE) for the electron-hole correlation function  $L$ :

$$L = L^0 + L^0 \Xi L, \quad (1)$$

where  $L^0$  describes the propagation of an independent particle and hole and  $\Xi$  is the electron-hole interaction kernel.

Within the *GW* approximation, the interaction kernel is given by  $\Xi = -V + W$ , where  $W$  and  $V$  are often referred to as the exchange and direct term, respectively. The former describes the screened Coulomb interaction between electrons and holes;  $V$  describes the exchange interaction of the electrons and holes. The matrix elements of the direct term are defined as

$$W_{cv\mathbf{k},c'v'\mathbf{k}'} = \int d^3r d^3r' \psi_{v\mathbf{k}}(\mathbf{r}) \psi_{v'\mathbf{k}'}^*(\mathbf{r}) W(\mathbf{r}, \mathbf{r}') \psi_{c\mathbf{k}}^*(\mathbf{r}') \psi_{c'\mathbf{k}'}(\mathbf{r}'), \quad (2)$$

where  $W(\mathbf{r}, \mathbf{r}')$  is the screened Coulomb potential,  $\psi_{c\mathbf{k}}$  and  $\psi_{v\mathbf{k}}$  are the conduction ( $c$ ) and valence ( $v$ ) quasi-particle wavefunctions at the point  $\mathbf{k}$ , respectively. Often, these wavefunctions are approximated by Kohn-Sham orbitals. The matrix elements of the exchange term are defined as

$$V_{cv\mathbf{k},c'v'\mathbf{k}'} = \int d^3r d^3r' \psi_{v\mathbf{k}}(\mathbf{r}) \psi_{c\mathbf{k}}^*(\mathbf{r}) v(\mathbf{r}, \mathbf{r}') \psi_{v'\mathbf{k}'}^*(\mathbf{r}') \psi_{c'\mathbf{k}'}(\mathbf{r}'), \quad (3)$$

where  $v(\mathbf{r}, \mathbf{r}')$  is the bare Coulomb potential. The BSE in Eq. 1 can be solved by diagonalizing the so-called Bethe-Salpeter Hamiltonian  $H^{BSE}$ . This Hamiltonian describes the coupling of independent-particle transitions from a valence orbital  $v$  to a conduction orbital  $c$  at a given  $\mathbf{k}$  with a different transition from  $v'$  to  $c'$  at  $\mathbf{k}'$ . The space spanned by all possible transitions at all  $\mathbf{k}$ -points is denoted as the transition space. In this space,  $H^{BSE}$  is defined as

$$H_{cv\mathbf{k},c'v'\mathbf{k}'}^{BSE} = \Delta E_{cv\mathbf{k},c'v'\mathbf{k}'} - W_{cv\mathbf{k},c'v'\mathbf{k}'} + V_{cv\mathbf{k},c'v'\mathbf{k}'}, \quad (4)$$

where  $\Delta E_{cv\mathbf{k},c'v'\mathbf{k}'} = [\epsilon_{c\mathbf{k}} - \epsilon_{v\mathbf{k}}] \delta_{cc'} \delta_{vv'} \delta_{\mathbf{k}\mathbf{k}'}$ , and  $\epsilon_{i\mathbf{k}}$  are the  $GW$  quasi-particle energies. The diagonalization of  $H^{BSE}$ :

$$H^{BSE} X_\lambda = E_\lambda X_\lambda, \quad (5)$$

yields the neutral excited states of the systems, with energy  $E_\lambda$ ;  $X_\lambda$  are the corresponding excited states.

The diagonalization of  $H^{BSE}$  in Eq. 5 for a defective solid yield all possible excitation energies, and in many cases it is a difficult task to separate excitations occurring between defect states and those between bulk states; in addition, such a diagonalization amounts to an unnecessary computational effort, if only excitation between defect states are of interest. We therefore employ a methodology that only targets the excitations between the localized defect orbitals whose energies lie in the band gap of the solid. These orbitals form a set of states that we denote as the *active space*  $A$ ; the remaining bulk states belong to the *environment*  $E$ . Using spaces  $A$  and  $E$ , the correlation function  $L$  is expressed as

$$L = \begin{pmatrix} L_{AA} & L_{AE} \\ L_{EA} & L_{EE} \end{pmatrix}, \quad (6)$$

where  $L_{AA}$  and  $L_{EE}$  are the correlation functions within the active space and environment, respectively. The blocks  $L_{AE}$  and  $L_{EA}$  describe the coupling of excitations in the active space and environment. The function  $L_{AA}$  is obtained from the Löwdin separation of Eq. 1 as

$$[L^{-1}]_{AA} = \left[ (L_0^{-1} - \Xi)_{AA} + \Xi_{AE} (L_0^{-1} - \Xi)_{EE}^{-1} \Xi_{EA} \right]^{-1}. \quad (7)$$

We assume that the matrix elements between the localized defect orbitals and bulk states of the environment are small compared to those between the defect orbitals themselves. Thus, the matrix elements of the direct terms  $H^d$  between active space and environment are assumed to be negligible compared to those of the exchange term  $H^x$ . We therefore assume  $\Xi_{AE} \approx -V$  and  $\Xi_{EA} \approx -V$ . Finally, a detailed and accurate treatment of the excitations in the environment is not desired, and we therefore approximate the interaction in the environment as  $\Xi_{EE} \approx -V$ . We therefore obtain

$$\begin{aligned} [L^{-1}]_{AA} &= \left[ (L_0^{-1} - W + V)_{AA} + V (L_0^{-1} + V)_{EE}^{-1} V \right]^{-1} \\ &= \left[ (L_0^{-1} - W + V)_{AA} + V_{AE} P^R(\omega) V_{EA} \right]^{-1} \\ &= \left[ (L_0^{-1})_{AA} - W_{AA} + [\mathbb{1} + V \chi^R(\omega)] V \right]^{-1} \\ &= \left[ (L_0^{-1})_{AA} - W_{AA} + (\epsilon_R^{-1}(\omega) V)_{AA} \right]^{-1} \end{aligned} \quad (8)$$

Here, we have expressed the polarizability  $\chi^R(\omega) = [L_0^{-1} + V]_{EE}^{-1}$  within the constrained random-phase approximation (cRPA), where transitions in the active space are not included in the definition of the polarizability. Using a constrained polarizability, we define a constrained dielectric function  $\epsilon_R(\omega)$  as  $\epsilon_R^{-1}(\omega) = \mathbb{1} + V \chi^R(\omega)$ . The final expression in Eq. 8 is easy to understand: To obtain the excitations within the active space, we only need to explicitly consider the active space transitions. The effect of all transitions within the environment, and between the environment and the active space, is included by screening the exchange interaction with the function  $\epsilon_R^{-1}(\omega)$ . We note that while the interaction kernel in Eq. 1 is static, a dynamical screening is present in Eq. 8, originating from the down-folding procedure. In practice, we approximate the screened exchange term as  $\bar{H}^x \approx \epsilon_R^{-1}(\omega = 0) V = W^R$ , analogous to the treatment of  $W$  in standard BSE implementations.

We can now combine Eq. 8 with Eq. 4 to obtain the Hamiltonian for the active space as

$$H_{cv\mathbf{k},c'v'\mathbf{k}'}^{eBSE} = \Delta E_{cv\mathbf{k},c'v'\mathbf{k}'} - W_{cv\mathbf{k},c'v'\mathbf{k}'} + W_{cv\mathbf{k},c'v'\mathbf{k}'}^R, \quad (9)$$

where now the indices  $c, v, c', v' \in A$ , i.e. they are limited to states in the active space.

	This work	Ref. [22]
$E_g$	7.43 (4.52)	7.26 (4.49)
$\Delta E_{\text{ion}}$	4.05 (2.00)	
$\Delta E_{\text{defect}}$	5.54 (3.23)	

TABLE II. Electronic structure of the neutral oxygen vacancy ( $F^0$  center) in MgO in the dilute limit. We report the bandgap  $E_g$ , the energy splitting between the occupied defect level and the CBM  $\Delta E_{\text{ion}}$ , and the energy splitting between the occupied and unoccupied defect levels  $\Delta E_{\text{defect}}$ . All calculations performed at the  $G_0W_0$ (PBE) level of theory and results shown in eV.

### A. Computational Details

We carried out DFT electronic-structure calculations and lattice relaxations using the Quantum Espresso code [25, 26] with optimized norm-conserving Vanderbilt (ONCV) pseudopotentials [27], 80 Ry cutoff, and supercells with the  $\Gamma$  point only. Embedded BSE excitation energies were then obtained from calculations [28] carried out with the WEST (Without Empty States) code, using matrix elements obtained from the WEST implementation of the Quantum Defect Embedding Theory (QDET) [29]. In the WEST code, a separable form of the screened Coulomb interaction  $W$  is obtained using the projected eigen-decomposition of the dielectric matrix (PDEP) [28, 30], which avoids the inversion and storage of large dielectric matrices. Importantly, any explicit summation over empty orbitals are eliminated using density functional perturbation theory (DFPT) [31] and iterative Lanczos methods [32, 33]. This implementation allows for MBPT calculations of defects in large supercells, containing hundreds of atoms.

## III. RESULTS

As mentioned in the introduction, an oxygen vacancy in MgO gives rise to four low-energy defect levels: A defect orbital with an  $s$ -like wavefunction and energy within the bandgap, and a threefold degenerate orbital with  $p$ -like wavefunction and energy just above the CBM. In the neutral charge state (denoted as  $V_{\text{O}}^0$  or  $F^0$ ), the in-gap orbital is doubly occupied; in the positive charge state ( $V_{\text{O}}^+$  or  $F^+$ ) it is singly occupied, and in the double-positive charge state ( $V_{\text{O}}^{2+}$  or  $F^{2+}$ ) it is empty. In order to fully characterize the electronic structure of the defect, we need to compute the bandgap  $E_g$ , the defect energy  $\Delta E_{\text{defect}}$  defined as the energy difference between the occupied in-gap and unoccupied defect orbitals above the CBM, and the three following ionization energies  $\Delta E_{\text{ion}}$ . For the neutral oxygen vacancy, the ionization energy  $\Delta E_{\text{ion}}^{(1)}$  is the energy difference between the CBM and the in-gap defect state. For the positively charged defect, only the spin-up channel of the defect state in the bandgap is occupied and two ionization channels are available:  $\Delta E_{\text{ion}}^{(0)}$  is the difference between the energy of the unoccupied defect state in the band-gap and that of the valence band maximum (VBM).  $\Delta E_{\text{ion}}^{(2)}$  is given by the difference between the CBM energy and that of the occupied in-gap state.

Figure 1 shows the convergence of  $G_0W_0$  quasi-particle energies as a function of the number of atoms in the supercell. As expected, the energy differences for both charge states converge as  $N_{\text{atoms}}^{-1}$ . In the dilute limit ( $N_{\text{atoms}} \rightarrow \infty$ ), we recover the bulk PBE and  $G_0W_0$  band gaps reported in the literature (see Table II).

We show in the following that understanding the defect excitation processes requires not only to compute energy levels but also to determine the localization of the respective wave-functions. To quantify the localization of defect orbitals, we define a localization factor  $L_V$  for each Kohn-Sham state  $\psi_i$ :

$$L_{\Omega'}[\psi_i] = \int_{\Omega' \in \Omega} |\psi_i(\mathbf{r})|^2 d^3r, \quad (10)$$

where  $\Omega'$  is a volume smaller than the supercell volume  $\Omega$ . The localization factor varies between zero (no charge density in the considered volume) and one (full localization), and to determine the degree of localization of a given orbital, we monitor the convergence of  $L$  as a function of cell size, for a chosen, constant value of  $\Omega'$ . Here the volume  $\Omega'$  includes the nearest-neighbor Mg atoms surrounding the vacancy. As seen in Fig. 1, the localization factor of the mid-gap state is around 0.75, demonstrating that the charge density is contained largely within the chosen cavity. We find that  $L$  is already well-converged for small supercells, even if the energy of the orbital changes significantly with supercell size. The  $p$ -like defect orbitals, on the other hand, are much less localized and the localization factor decreases slowly with supercell size, slower than  $N_{\text{atoms}}^{-1}$ .

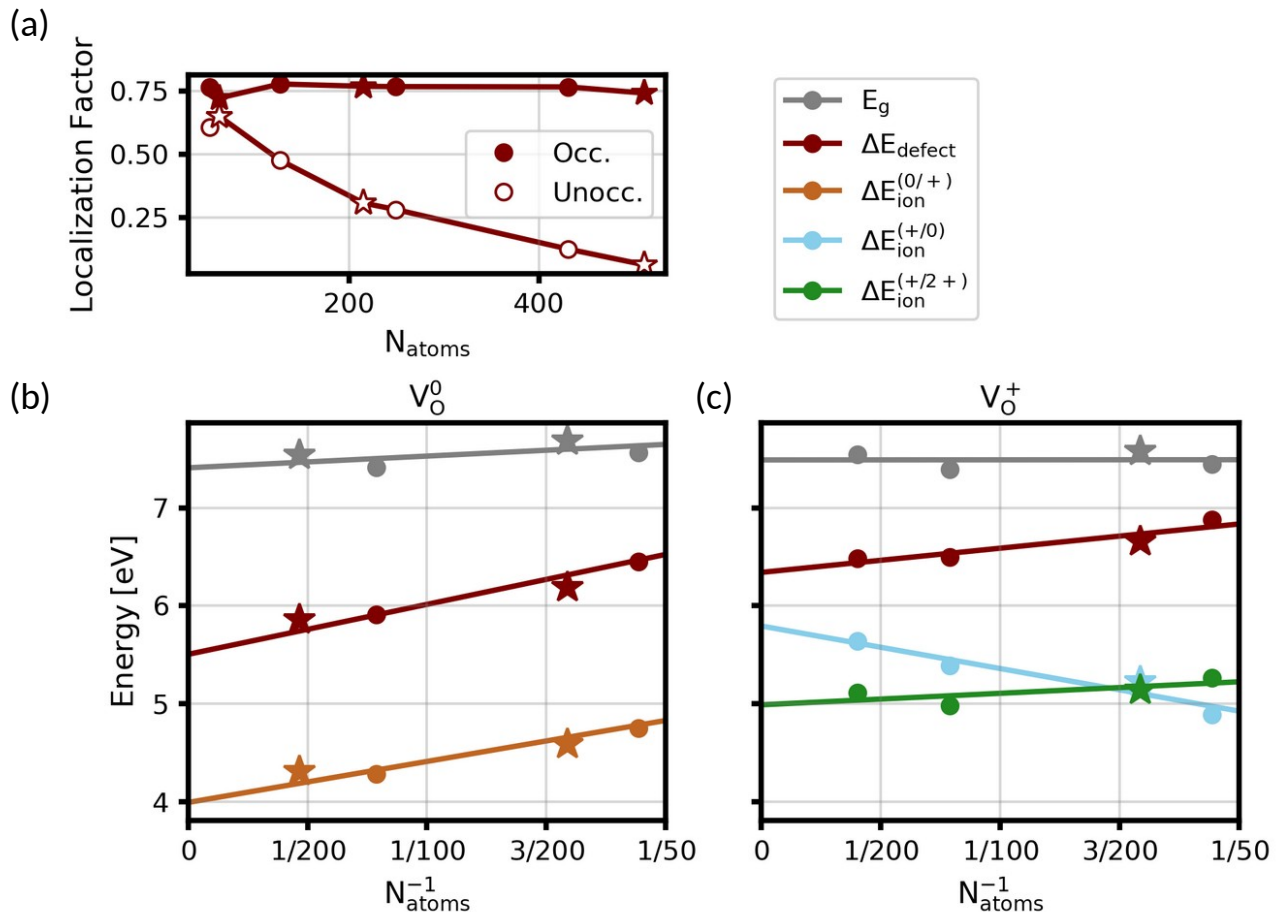


FIG. 1. a) Localization factor for the occupied (full symbols) and unoccupied (open symbols) defect orbitals in the neutral oxygen vacancy in MgO ( $V_{\text{O}}^0$  or F center). Circles and stars denote results obtained with supercells of the primitive and conventional supercell, respectively. Ionization energies  $\Delta E_{\text{ion}}$  and defect energies  $\Delta E_{\text{defect}}$  for b) the neutral and c) the positive charge state determined from  $G_0W_0$  quasi-particle energies. All energies are defined in the text.

### A. Absorption by the neutral oxygen vacancy

Absorption of light by the  $V_{\text{O}}^0$  defect can trigger a number of different excitation processes. Here we focus on three processes with the lowest excitation energies. (i) An electron from the mid-gap state is excited to the CBM, thus ionizing the defect. The Coulomb attraction between the excited electron and the ionized defect can bind the excited electron to the defect, leading to a so-called *bound exciton* (sometimes also denoted as a defect-bound exciton). (ii) Alternatively, an electron can be excited from the occupied defect orbital to the threefold degenerate unoccupied defect orbital. We denote this process as a *defect excitation*, as the final state of the absorption is an excited state of the defect without a change of the charge state. (iii) An electron can also be excited from the valence-band maximum (VBM) to the conduction-band minimum (CBM). As in process (i), the attraction between the excited electron and the valence hole leads to the formation of an exciton, which in this case we call *free exciton*. We note that the excitation energy of the free exciton should, in the dilute limit, be identical to the one obtained from bulk calculations without any defect.

The energies of the transitions (i)-(iii) as a function of the supercell size are shown in Fig. 2. We find that the defect-excitation energy decreases as  $N_{\text{atoms}}^{-1}$ , where  $N_{\text{atoms}}$  is the number of atoms in the supercell. The free-exciton energy, on the other hand, increases with increasing supercell size. Finally, the bound-exciton energy initially decreases with increasing supercell size, but then increases for larger supercells. For the largest supercell with 249 atoms, we obtain a bound-exciton energy of 3.7 eV, a defect-excitation energy of 4.8 eV, and a free-exciton energy of 6.8 eV. We find that the free-exciton energy is in excellent agreement with the corresponding energy of 6.82 eV obtained from GW-BSE calculations for the pristine lattice [22]. This indicates that the largest supercells used here are sufficient to

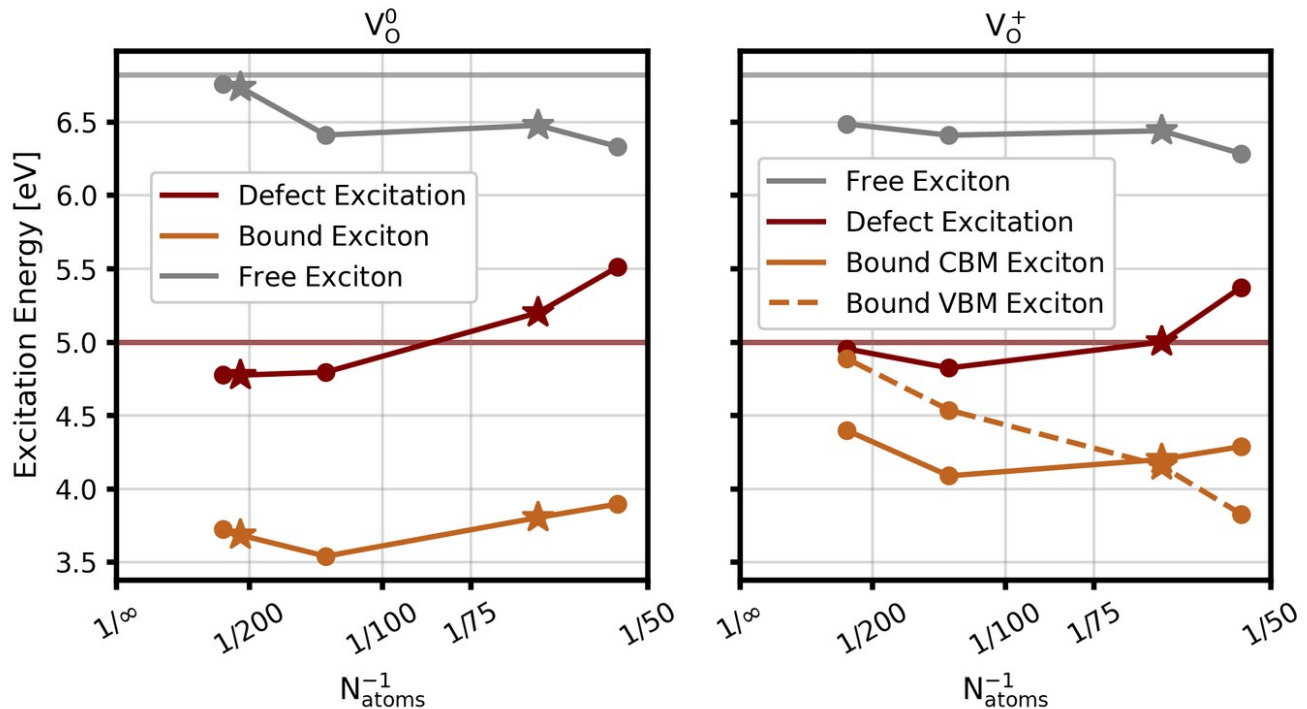


FIG. 2. Defect-excitation (red), bound-exciton (orange), and free-exciton (grey) excitation energies for the neutral oxygen vacancy ( $F^0$  center) in MgO as a function of the number of atoms  $N_{\text{atoms}}$  in the supercell. Circles denote results obtained with primitive supercells, and stars those obtained with conventional ones.

reproduce the pristine bulk electronic structure. The computed defect-excitation energy of 4.8 eV underestimates the experimental value of 5.0 eV. This underestimate stems from the density functional chosen to obtain single particle wavefunctions used as a starting point of  $GW$  calculations. This can be understood by comparing results where the DFT single particle wavefunctions are obtained from PBE and hybrid functionals, in particular the dielectric-dependent hybrid (DDH) functional [34]. The defect excitation energies computed with DDH consistently increase by 430 meV, compared to PBE, leading to a defect excitation energy of 5.23 eV and bound exciton energy of 4.13 eV. For more details, see Ref. [35].

### 1. Momentum Matrix Elements

As discussed in the previous section, our first-principles calculations predict that the absorption by the neutral oxygen vacancy leads to excitations between the localized defect orbitals, not to the formation of a bound exciton. The momentum matrix elements of the different excitations further confirms this finding. In Fig. 3 we show the momentum matrix elements as a function of the number of atoms in the supercell. The momentum matrix elements for the free exciton, *i.e.* the transition from VBM to CBM, increase with increasing supercell size. The non-vanishing matrix elements are consistent with the results of previous BSE calculations for pristine MgO [22], which reported the presence of a bright exciton (free exciton).

However, we find that the matrix element for the bound exciton vanishes for all supercell sizes, as both the initial state (the localized defect orbital) and the final state of the transition (the CBM) have  $s$ -like character. The vanishing matrix element indicates that the formation of the bound exciton is dipole-forbidden and therefore light absorption

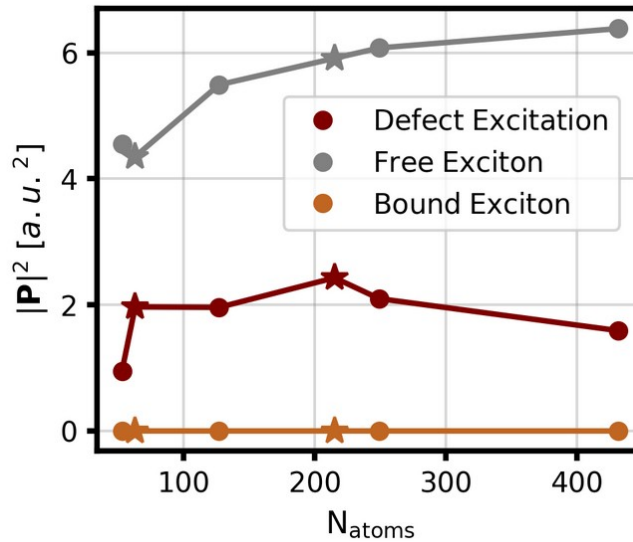


FIG. 3. Momentum matrix elements of the defect-excitation (red), bound-exciton (orange), and free-exciton (grey) for the neutral oxygen vacancy (or  $F^0$  center) in MgO as a function of the number of atoms  $N_{\text{atoms}}$  in the supercell. Circles (stars) denote results obtained with primitive supercells (conventional ones).

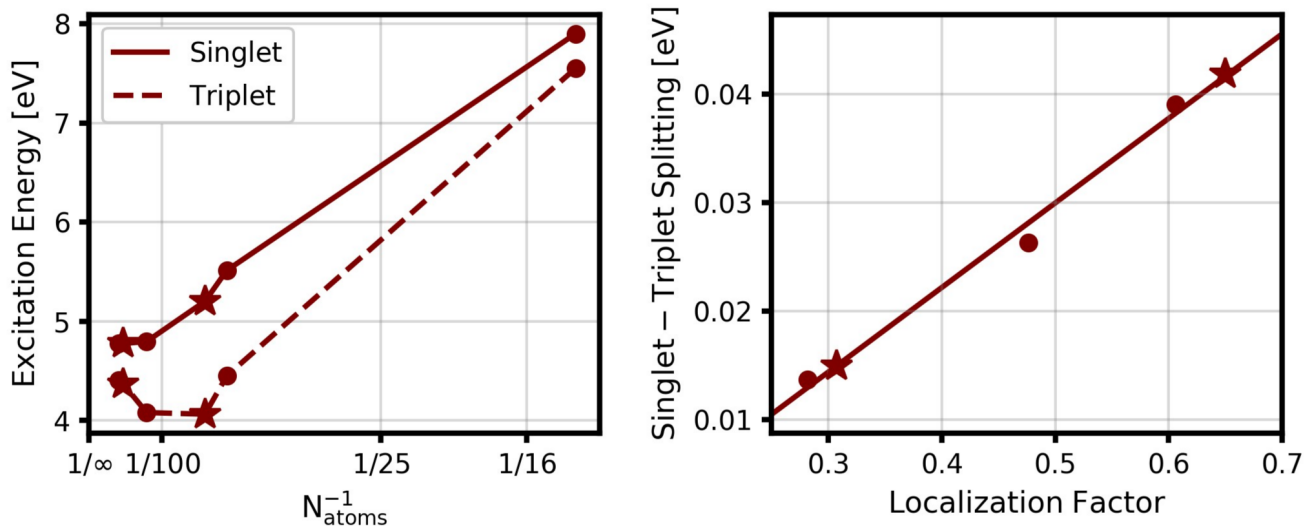


FIG. 4. Left: Singlet (solid line) and triplet (dotted line) excitation energy of the  $F^0$  center in MgO. Circles denote primitive supercells, stars denote conventional ones. Right: The singlet-triplet splitting as a function of the localization factor of the unoccupied defect orbitals.

between states that would give rise to a bound exciton is unlikely.

Excitations between defect states, on the other hand, are dipole-allowed, as the initial and final states have  $s$ - and  $p$ -character, respectively. We find that the matrix elements for these excitations converge quickly as a function of the supercell size, and while these matrix elements are smaller than those for the free exciton, they are significantly larger than those for the dipole-forbidden bound exciton.

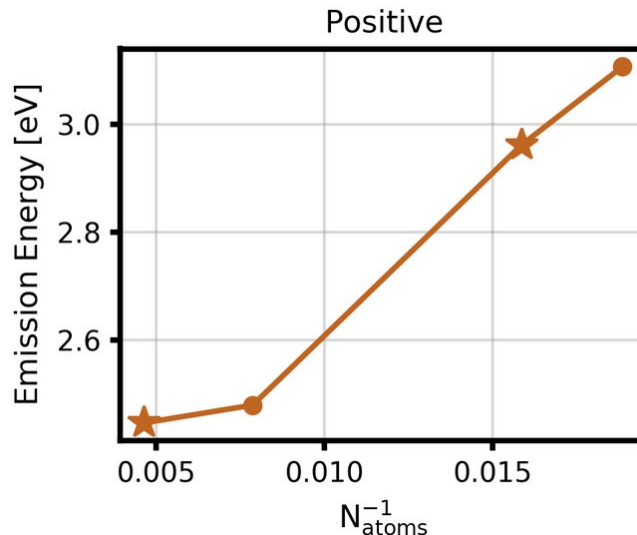


FIG. 5. Electron capture of the neutral oxygen vacancy  $V_{\text{O}}^+$  as a function of the number of atoms in the supercell. Circles (stars) indicate results obtained primitive (conventional) supercells.

### B. Emission from the Triplet Excited State of the neutral oxygen vacancy

The emission of the neutral oxygen vacancy (or  $F^0$  center) has repeatedly been attributed to triplet excited states. We therefore show in Fig. 4 the singlet and triplet excitation energies of the  $F^0$  center. We find that the triplet excitation energy changes non-monotonically as a function of  $N_{\text{atoms}}$ . It decreases by about 3.5 eV as the supercell size increases from 15 ( $2 \times 2 \times 2$  primitive) to 63 ( $2 \times 2 \times 2$  conventional) atoms; however, a further increase of the supercell leads to an increase of the triplet excitation energy. The non-monotonic behavior originates from the different convergence as a function of cell size, of different terms entering the BSE Hamiltonian: The  $G_0W_0$  energy differences decrease as  $N_{\text{atoms}}^{-1}$  (see Fig. 1), and the decrease in the direct and exchange term is instead proportional to the localization factor  $L$  of the defect orbital. For the triplet excitations, the exchange interaction vanishes and the interplay between the different convergence rates is responsible for the non-monotonic behavior shown in Fig. 4. For the singlet excitations, the competition between the convergence of the attractive direct and repulsive exchange terms leads to an overall convergence close to  $N_{\text{atoms}}^{-1}$ . An intuitive interpretation of our findings is that the singlet-triplet splitting decreases due to a decrease of the exchange term, as the defect orbital becomes more delocalized. We emphasize that due to the non-monotonic convergence of the triplet-excitation energy, it is not possible to extrapolate the singlet-triplet splitting to the dilute limit. We argue that the splitting of 0.33 eV, which we determine from the 249-atom supercell calculation is the upper limit to the value one would find in the dilute limit. This upper limit is significantly smaller than the value of 1.62 eV obtained from equation of motion coupled-cluster (EOM-CC) calculations. The latter employed an extrapolation to the dilute limit from small supercell calculations (with up to  $\mathbf{xx}$  atoms), assuming a  $N_{\text{atoms}}^{-1}$  convergence of both singlet and triplet excitation energies.

### C. Emission from Electron Capture of the neutral oxygen vacancy

The emission due to the hole capture at a  $V_{\text{O}}^+$  defect has been proposed as an alternative to the emission occurring from the excited triplet state of the  $V_{\text{O}}^0$ . In detail, the proposed, alternative process is the following: The absorption of a  $V_{\text{O}}^0$  leads to an excited defect state with the same charge state. The excited electron is then transferred to the conduction band minimum, ionizing the defect to  $V_{\text{O}}^+$ . The observed emission would then originate from the capture of an electron by  $V_{\text{O}}^+$  that then transitions to the neutral charge state, and occurs due to a  $e^{CBM} + V_{\text{O}}^+ \rightarrow V_{\text{O}}^0$  transition. In Figure 5, we show the calculated emission energy as a function of the number of atoms in the supercells. We find that the emission energy decreases with supercell size but does not converge as  $N_{\text{atoms}}^{-1}$ ; rather it is already converged

for a supercell with 127 atoms, yielding an emission energy of about 2.5 eV, below the experimentally reported value of 3.2 - 3.4 eV [19, 20]. From our analysis of the error of the PBE functional for the computed absorption energies of the neutral oxygen vacancy, we estimate that the emission energy may increase by  $\simeq 430$  meV when using the DDH functional, yielding a value of 2.93 eV, in better agreement with experiment.

#### IV. CONCLUSIONS

In summary, we presented a detailed study of the electronic structure of oxygen vacancies in MgO, using an embedded BSE methodology (eBSE) originally proposed in Ref. [24] for 2D systems and applied here for the first time to a 3D material. Our implementation of eBSE in the WEST code is based on concepts and algorithms developed in the context of quantum embedding theory [29, 36, 37]. We investigated competing photoionization and photo-excitation processes and obtained accurate energies for both processes, through an accurate and consistent treatment of excitation involving delocalized and localized states. Importantly, we solved a controversy present in the literature regarding the nature of absorption and emission processes. We find that the absorption detected experimentally at 5 eV is due to the photo-excitation of the neutral oxygen vacancy as predicted by Refs. [13, 15, 18], but contrary to the reports of Refs. [14, 16, 17] and that the photoemission occurs through a ionization process in agreement with Refs. [14, 16, 17] but contrary to Ref. [18]. We note that using an accurate and consistent level of theory for absorption and emission *and* conducting finite size scaling tests are both critical ingredients of our computational strategy. The protocol presented here to study oxygen vacancies can be applied to any point defect, which has nearly-degenerate photo-ionization and photo-excitation energies, and any defect that has defect orbitals close or above the conduction band maximum.

#### ACKNOWLEDGMENTS

We thank Marco Govoni, Nan Sheng, and Yu Jin for useful discussions. This work was supported by the computational materials science center Midwest Integrated Center for Computational Materials (MICCoM) for the implementation of the embedded GW-BSE method in the WEST code, and by AFOSR Grant No. FA9550-19-1-0358 for the application of the code to study the F center in MgO. MICCoM is part of the Computational Materials Sciences Program funded by the U.S. Department of Energy, Office of Science, Basic Energy Sciences, Materials Sciences, and Engineering Division through the Argonne National Laboratory, under Contract No. DE-AC02-06CH11357. This research used resources of the National Energy Research Scientific Computing Center (NERSC), a DOE Office of Science User Facility supported by the Office of Science of the U.S. Department of Energy under Contract No. DE-AC02-05CH11231, and resources of the University of Chicago Research Computing Center.

- 
- [1] F. Gunkel, D. V. Christensen, Y. Z. Chen, and N. Pryds, Oxygen vacancies: The (in)visible friend of oxide electronics, *Appl. Phys. Lett.* **116**, 120505 (2020).
  - [2] B. Taudul, E. N. Montebalco, U. Halisdemir, D. Lacour, F. Schleicher, F. Montaigne, E. Beaurepaire, S. Boukari, M. Hehn, M. Alouani, and M. Bowen, Tunneling Spintronics across MgO Driven by Double Oxygen Vacancies, *Adv. Electron. Mater.* **3**, 1600390 (2017).
  - [3] F. Schleicher, U. Halisdemir, D. Lacour, M. Gallart, S. Boukari, G. Schmerber, V. Davesne, P. Panissod, D. Halley, H. Majjad, Y. Henry, B. Leconte, A. Boulard, D. Spor, N. Beyer, C. Kieber, E. Sternitzky, O. Cregut, M. Ziegler, F. Montaigne, E. Beaurepaire, P. Gilliot, M. Hehn, and M. Bowen, Localized states in advanced dielectrics from the vantage of spin- and symmetry-polarized tunnelling across MgO, *Nature Comm.* **5**, 4547 (2014).
  - [4] G. X. Miao, Y. J. Park, J. S. Moodera, M. Seibt, G. Eilers, and M. Münzenberg, Disturbance of Tunneling Coherence by Oxygen Vacancy in Epitaxial Fe/MgO/Fe Magnetic Tunnel Junctions, *Phys. Rev. Lett.* **100**, 246803 (2008).
  - [5] J. P. Velez, K. D. Belashchenko, S. S. Jaswal, and E. Y. Tsybal, Effect of oxygen vacancies on spin-dependent tunneling in Fe/MgO/Fe magnetic tunnel junctions, *Appl. Phys. Lett.* **90**, 072502 (2007).
  - [6] I. A. Popov, E. Jimenez-Izal, A. N. Alexandrova, and A. I. Boldyrev, Multicenter Bonding Effects in Oxygen Vacancy in the Bulk and on the Surface of MgO, *J. Chem. Phys. C* **122**, 11933 (2018).
  - [7] M. Kulichenko, N. Fedik, D. Steglenko, R. M. Minyaev, V. I. Minkin, and A. I. Boldyrev, Periodic F-defects on the MgO surface as potential single-defect catalysts with non-linear optical properties, *Chem. Phys.* **532**, 110680 (2020).
  - [8] X. D. Peng, D. A. Richards, and P. C. Stair, Surface composition and reactivity of lithium-doped magnesium oxide catalysts for oxidative coupling of methane, *J. Catal.* **121**, 99 (1990).
  - [9] Y. C. Sharma, B. Singh, and J. Korstad, Latest developments on application of heterogenous basic catalysts for an efficient and eco friendly synthesis of biodiesel: A review, *Fuel* **90**, 1309 (2011).

- [10] Y. Hinuma, T. Toyao, T. Kamachi, Z. Maeno, S. Takakusagi, S. Furukawa, I. Takigawa, and K.-i. Shimizu, Density Functional Theory Calculations of Oxygen Vacancy Formation and Subsequent Molecular Adsorption on Oxide Surfaces, *J. Chem. Phys. C* **122**, 29435 (2018).
- [11] R. I. Eglitis, M. M. Kukulja, E. A. Kotomin, A. Stashans, and A. I. Popov, Semi-empirical simulations of the electron centers in MgO crystal, *Comp. Mater. Sci.* **5**, 298 (1996).
- [12] B. X. Shi, V. Kapil, A. Zen, J. Chen, A. Alavi, and A. Michaelides, General embedded cluster protocol for accurate modeling of oxygen vacancies in metal-oxides, *J. Chem. Phys.* **156**, 124704 (2022).
- [13] A. Gallo, F. Hummel, A. Imler, and A. Grüneis, A periodic equation-of-motion coupled-cluster implementation applied to F-centers in alkaline earth oxides, *J. Chem. Phys.* **154**, 064106 (2021).
- [14] E. Ertekin, L. K. Wagner, and J. C. Grossman, Point-defect optical transitions and thermal ionization energies from quantum Monte Carlo methods: Application to the F-center defect in MgO, *Phys. Rev. B* **87**, 155210 (2013).
- [15] C. Sousa and F. Illas, On the accurate prediction of the optical absorption energy of F-centers in MgO from explicitly correlated ab initio cluster model calculations, *J. Chem. Phys.* **115**, 1435 (2001).
- [16] P. Rinke, A. Schleife, E. Kioupakis, A. Janotti, C. Rödl, F. Bechstedt, M. Scheffler, and C. G. Van de Walle, First-Principles Optical Spectra for F Centers in MgO, *Phys. Rev. Lett.* **108**, 126404 (2012).
- [17] S. Tosoni, D. Fernandez Hevia, J. Perez Peña, and F. Illas, Prediction of optical properties of F centers in oxides from quasiparticle excitations, *Phys. Rev. B* **85**, 115114 (2012).
- [18] J. Strand, S. K. Chulkov, M. B. Watkins, and A. L. Shluger, First principles calculations of optical properties for oxygen vacancies in binary metal oxides, *J. Chem. Phys.* **150**, 044702 (2019).
- [19] Y. Chen, R. T. Williams, and W. A. Sibley, Defect Cluster Centers in MgO, *Phys. Rev.* **182**, 960 (1969).
- [20] L. A. Kappers, R. L. Kroes, and E. B. Hensley,  $F^{+}$  and  $F'$  Centers in Magnesium Oxide, *Phys. Rev. B* **1**, 4151 (1970).
- [21] B. Henderson, R. D. King, and A. M. Stoneham, The temperature dependence of the F band in magnesium oxide, *J. Phys. C* **1**, 586 (1968).
- [22] V. Begum, M. E. Gruner, C. Vorwerk, C. Draxl, and R. Pentcheva, Theoretical description of optical and x-ray absorption spectra of MgO including many-body effects, *Phys. Rev. B* **103**, 195128 (2021).
- [23] W. Gao, F. H. da Jornada, M. Del Ben, J. Deslippe, S. G. Louie, and J. R. Chelikowsky, Quasiparticle energies and optical excitations of 3C-SiC divacancy from GW and GW plus Bethe-Salpeter equation calculations, *Phys. Rev. Materials* **6**, 036201 (2022).
- [24] D. Y. Qiu, F. H. da Jornada, and S. G. Louie, Solving the Bethe-Salpeter equation on a subspace: Approximations and consequences for low-dimensional materials, *Phys. Rev. B* **103**, 045117 (2021).
- [25] P. Giannozzi, S. Baroni, N. Bonini, M. Calandra, R. Car, C. Cavazzoni, D. Ceresoli, G. L. Chiarotti, M. Cococcioni, I. Dabo, A. D. Corso, S. de Gironcoli, S. Fabris, G. Fratesi, R. Gebauer, U. Gerstmann, C. Gougoussis, A. Kokalj, M. Lazzeri, L. Martin-Samos, N. Marzari, F. Mauri, R. Mazzarello, S. Paolini, A. Pasquarello, L. Paulatto, C. Sbraccia, S. Scandolo, G. Sclauzero, A. P. Seitsonen, A. Smogunov, P. Umari, and R. M. Wentzcovitch, QUANTUM ESPRESSO: A modular and open-source software project for quantum simulations of materials, *J. Phys. Condens. Matter.* **21**, 395502 (2009).
- [26] P. Giannozzi, O. Andreussi, T. Brumme, O. Bunau, M. B. Nardelli, M. Calandra, R. Car, C. Cavazzoni, D. Ceresoli, M. Cococcioni, N. Colonna, I. Carnimeo, A. D. Corso, S. de Gironcoli, P. Delugas, R. A. DiStasio, A. Ferretti, A. Floris, G. Fratesi, G. Fugallo, R. Gebauer, U. Gerstmann, F. Giustino, T. Gorni, J. Jia, M. Kawamura, H.-Y. Ko, A. Kokalj, E. Küçükbenli, M. Lazzeri, M. Marsili, N. Marzari, F. Mauri, N. L. Nguyen, H.-V. Nguyen, A. Otero-de-la-Roza, L. Paulatto, S. Poncé, D. Rocca, R. Sabatini, B. Santra, M. Schlipf, A. P. Seitsonen, A. Smogunov, I. Timrov, T. Thonhauser, P. Umari, N. Vast, X. Wu, and S. Baroni, Advanced capabilities for materials modelling with Quantum ESPRESSO, *J. Phys. Condens. Matter.* **29**, 465901 (2017).
- [27] M. Schlipf and F. Gygi, Optimization algorithm for the generation of ONCV pseudopotentials, *Comput. Phys. Commun.* **196**, 36 (2015).
- [28] M. Govoni and G. Galli, Large Scale GW Calculations, *J. Chem. Theory. Comput.* **11**, 2680 (2015).
- [29] N. Sheng, C. Vorwerk, M. Govoni, and G. Galli, Green's Function Formulation of Quantum Defect Embedding Theory, *J. Chem. Theory. Comput.* **18**, 3512 (2022).
- [30] H. F. Wilson, F. Gygi, and G. Galli, Efficient iterative method for calculations of dielectric matrices, *Phys. Rev. B* **78**, 113303 (2008).
- [31] S. Baroni, S. de Gironcoli, A. Dal Corso, and P. Giannozzi, Phonons and related crystal properties from density-functional perturbation theory, *Rev. Mod. Phys.* **73**, 515 (2001).
- [32] P. Umari, G. Stenuit, and S. Baroni, GW quasiparticle spectra from occupied states only, *Phys. Rev. B* **81**, 115104 (2010).
- [33] H.-V. Nguyen, T. A. Pham, D. Rocca, and G. Galli, Improving accuracy and efficiency of calculations of photoemission spectra within the many-body perturbation theory, *Phys. Rev. B* **85**, 081101 (2012).
- [34] J. H. Skone, M. Govoni, and G. Galli, Self-consistent hybrid functional for condensed systems, *Phys. Rev. B* **89**, 195112 (2014).
- [35] See Supplemental Material at [URL will be inserted by publisher] for a discussion of the starting-point dependence of embedded BSE calculation.
- [36] H. Ma, N. Sheng, M. Govoni, and G. Galli, First-principles studies of strongly correlated states in defect spin qubits in diamond, *Phys. Chem. Chem. Phys.* **22**, 25522 (2020).
- [37] H. Ma, N. Sheng, M. Govoni, and G. Galli, Quantum Embedding Theory for Strongly Correlated States in Materials, *J. Chem. Theory. Comput.* **17**, 2116 (2021).